Analytical Maximum Torque per Volt control strategy of an IPMSM with very low battery voltage

Alberto Sanz [1], Estanis Oyarbide [1], Rubén Gálvez [2], Carlos Bernal [1], Pilar Molina [1], Igor San Vicente[3]

[1] Aragon Institute for Engineering Research, University of Zaragoza, Spain
[2] Epic Power Converters
[3] Fagor Electrónica S Coop

E-mail: albertosanz@unizar.es

ET Electric Power Applications(2019), 13 (7):1042
http://dx.doi.org/10.1049/iet-epa.2018.5469

Abstract: The operation of an IPMSM motor included in an Electric Power Steering system is related to two demanding requirements: a) the low voltage DC source pushes the motor to a deep flux weakening region, and, b) the motor is so optimized that it can withstand only some few cycles at nominal torque. Because of that, Maximum Torque Per Ampere (MTPA) and Maximum Torque Per Volt (MTPV) current reference generation strategies are commonplace in this type of applications. Most of the published MTPA or MTPV strategies are applied to standard voltage motors, so stator resistance is typically neglected, leading to simpler equations. Other works consider the stator resistance but, as the resulting equations are complex, look-up tables or numerically adjusted polynomials are employed in current generation tasks.
This work presents analytical expressions allowing the exact computing of current references. These expressions include stator resistances. The battery voltage is considered as an input variable, together with motor speed and reference torque, and direct and quadrature current references are the output variables. Contrary to look-up tables or numerically adjusted polynomials, the proposed expressions can take into account any parameter variation during real-time operation. Simulation and experimental results validate the proposed approach.

1. Introduction

Interior Permanent Magnet Synchronous Motors (IPMSM) are widely used in on-board systems (e.g. automotive and aero spatial sectors) due to their high performance in a compact and robust design. In this work, the IPMSM is part of an Electric Power Steering (EPS) for small cars.

The implemented control strategy quickly establishes the operation conditions that allow the motor to provide the torque required by the user. This is done through a vector current control loop and a current reference generator block (Fig. 1). This article proposes a novel strategy on the current reference generation approach.

An EPS needs to deal with the overheating of the motor and electronic boards, which depends on motor currents. That is why EPS systems need to determine the amplitude and position of the minimum current that can provide the required torque, exploiting the so-called Maximum Torque Per Ampere (MTPA) strategy.

The highest difficulty appears at high speeds, where field-weakening strategies are required due to voltage saturation, requiring Maximum Torque Per Volt (MTPV) strategies.

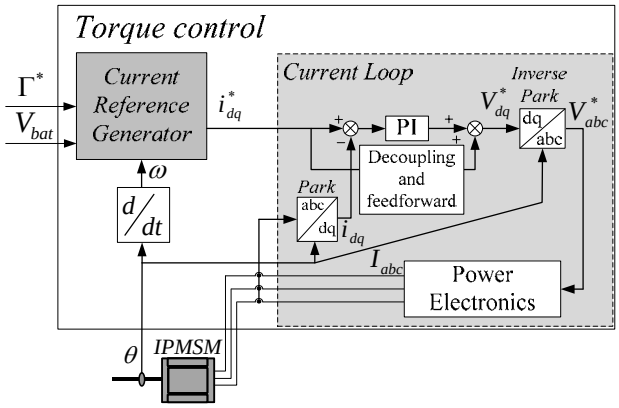

Fig. 1. *Block diagram showing the IPMSM control*

This motor has inserted magnets, so it is possible to increase the torque capacity of the EPS by taking advantage of the "reluctant torque". However, this complicates the analytical relationships of the motor.

Moreover, the voltage range extends from 6V to 18V, while motor currents are high (100A). Thus, unlike with motors operating at industrial voltage levels, phase resistances must be considered in voltage equations. These problems have been previously studied using different approaches:

- Most of them use of look-up-tables and neglect the phase resistance ($R \cong 0$) [1-7]. They are model-based and therefore they are dependent on the machine parameters.
- Some works try to avoid look-up tables by means of numerical approximations [8-12]. References [8] and [9] neglect the phase resistance. References [10], [11] take into account phase resistances and the reluctant torque but do not operate in the MTPV region, so the most challenging region in low-voltage scenarios is not considered. Besides, [11] states that the intersecting point of the required torque curve with the voltage limit does not have an analytical expression. [12] does not operate in the MTPV region either.
- Other authors calculate current references using analytical expressions, but do not take into account the phase resistance [13], [14] or do not operate in the flux weakening region [15].
- Nowadays, some works focus on MTPA and flux weakening strategies that are independent from machine parameters. Some of them propose universal lookup tables [16], others exploit virtual signal injection strategies [17], and there are power perturbation approaches [18]. In any case, they neither provide the exact value of the minimum current leading to the torque reference in all the operating regions, nor operate in the MTPV path.

In this work, the development of the current reference generation block was carried out considering the reluctant torque ($L_d \neq L_q$) and phase resistances. The battery voltage has been considered as a third input variable, together with

torque reference and motor speed. Contrary to what is stated in [11], an analytical expression of the intersecting point of the required torque curve with the voltage limit is proposed. The current reference computation is carried out through an algorithm based on the exact motor analytical expressions, making no use of look-up-tables, numerical approximations or simplifications in any case.

Motor inductances L_d and L_q, motor resistance R and rotor flux ϕ_{pm} are external parameters that can evolve during real time execution of the algorithm. As the current references are computed *on-line,* contrary to look-up-tables based methods, it is possible to exploit *on-line* parameter estimation strategies, which leads to optimal current references under any operation condition. In literature, there are many thorough and successful parameter estimation strategies [19], [20], [21]. The object of this work is the development of an enhanced current references generation strategy.

2. Proposed Strategy

The goal of the Current Reference Generation strategy is to identify the best-suited current-reference that assures the required torque. Depending on the machine operation mode (temperature and speed) and on the voltage level of the battery, the maximum available current will vary, so the required torque will be reachable or not. If the reference torque is reachable, the best-suited current will be the minimum current assuring the required torque, thus, the current with minimum thermal impact. On the other hand, if the required torque is not reachable, the best-suited current will be the current leading to the maximum possible torque, thus minimizing the torque error. First, it is interesting to determine the best-suited current without considering any type of current limitation. Next, the impact of current limitations due to thermal or operational restrictions will be studied.

2.1. Unconstrained current: MTPA path

The torque of a PMSM is given by equation (1),

$$\Gamma(i_d, i_q) = \frac{3}{2} p i_q \left[\phi + (L_d - L_q) i_d \right] \tag{1}$$

where p is the number of pole-pairs, ϕ is the permanent-magnet flux, L_d and L_q are the direct and quadrature inductances respectively and i_d and i_q are the direct and quadrature currents, respectively. As torque depends on currents, torque limits will be related to current limits. As a starting point, we suppose that there are not restrictions in current values. As it can be derived from (1), there are infinite i_d-i_q current sets capable of providing a given torque. Thus, per each required torque a "constant torque trajectory" containing all the possible i_d-i_q points can be drawn in the d-q current plane, see the example of Fig. 2. In this example the required currents for 1Nm, 2Nm and 3Nm (and its negative values) are drawn. In the 2Nm case, five current vectors out of all infinite possible current vectors are also shown. As it can be observed, among all possible current vector values, i_{s3} is the smallest current vector leading to a 2Nm torque. Thus, i_{s3} will be the choice if a 2Nm torque is required. The Maximum Torque Per Ampere trajectory (MTPA) contains the set of minimum required currents i_s leading to the required torque values. Considering the amplitude of the current (2) and the torque equation (1) the analytical expression of the MTPA trajectory (3) can be obtained.

$$i_s = \sqrt{i_d^2 + i_q^2} \tag{2}$$

$$i_d(i_q) = \frac{-\varphi + \sqrt{\varphi^2 + 4(L_d - L_q)^2 i_q^2}}{2(L_d - L_q)} \tag{3}$$

The MTPA i_d value for a given torque is obtained by solving i_q in equation (1) and replacing it in equation (3).

$$i_d = \frac{-\phi + \sqrt{\phi^2 + 4(L_d - L_q)^2 \left(\frac{\Gamma}{\frac{3}{2} p \left(\phi + (L_d - L_q) i_d \right)} \right)^2}}{2(L_d - L_q)} \tag{4}$$

A fourth degree polynomial in i_d depending on the torque is obtained, see equation (29) in appendix 6.1. It is easy to identifythe correct solution as the only one with logical values, shown in equation (5). Replacing (5) in (1) it is straightforward to get i_q (6).

$$i_d = -\frac{t_2}{4t_1} - \frac{p_4}{2} - \frac{\sqrt{p_5 - p_6}}{2} \tag{5}$$

$$i_q = \frac{\Gamma_{ref}}{1.5\, p(\phi + i_d (L_d - L_q))} \tag{6}$$

Where t_1, t_2, p_4, p_5 and p_6 are coefficients that depend on L_d, L_q, ϕ and Γ_{ref}, see Appendix 6.1.

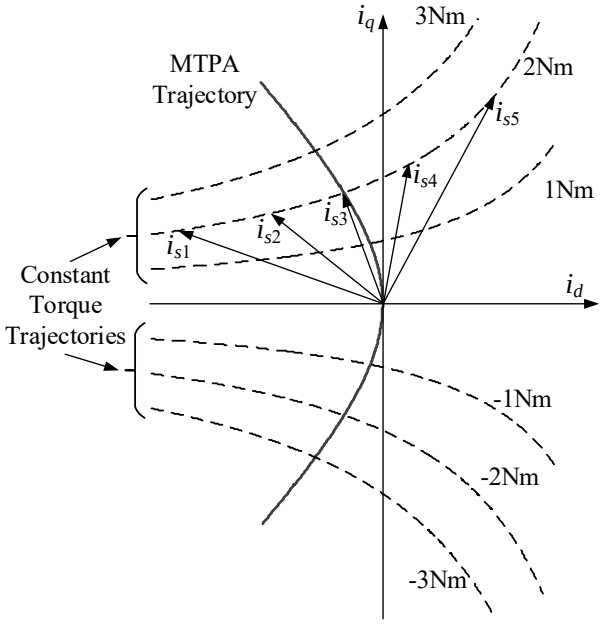

Fig. 2*. Constant torque and MTPA trajectories*

2.2. Current limit due to thermal restrictions

The current limit ($i_s = i_{smax}$) circle in the i_d-i_q plane is depicted in Fig. 4, where the demagnetization limit is also represented. If this last limit is exceeded (even for a small period of time), the magnets become permanently demagnetized.

2.3. Current limit due to voltage restriction

The electromotive force increases with speed, so the higher the speed, the higher the required voltage for a given current. Once the maximum available voltage is reached, the current must decrease with speed. Given any battery voltage, V_{BAT}, the voltage restriction can be expressed as:

$$v_d^{\,2} + v_q^{\,2} \le V_{SM}^2 = \left(\frac{V_{BAT}}{\sqrt{3}}\right)^2 \tag{7}$$

The voltage restriction (7) can be expressed in terms of i_d-i_q currents (8), according to the equivalent model of the IPMSM machine.

$$(Ri_d - \omega L_q i_q)^2 + \left[Ri_q + \omega(L_d i_d + \phi)\right]^2 = V_{SM}^2 \tag{8}$$

Where ω is the electrical speed. If phase resistance is neglected expression (8) equals an ellipse equation, but when phase resistance is considered, voltage ellipses are deformed. This is the case of Fig. 3 (c), where the major axis of the ellipse is no longer parallel to the i_d axis. This misalignment increases as phase inductance decreases.Fig. 3 (a) and (b) depict the voltage limits with and without considering phase resistances for two different IPMSM (parameters stated in Tables 1 and 2, in appendix 6.5). Both them are operating in the first and third quadrants, with V_{BAT} = 9 V, ω_1= ±400 rad/s and ω_2= ±800rad/s. Both machines have similar phase resistances, but the inductance of A machine is half that of the B machine. The modelling error on the voltage limit caused when the resistance is neglected is greater for the A motor. Moreover, as the speed increases, the centre of the ellipse moves to the left-down side of the i_{dq} plane: the lower the inductance, the larger the displacement, see Fig. 3 (c). Fig. 3 (c) shows the voltage limits for the first and fourth quadrants, ω_1= 400 rad/s and ω_2= 800rad/s, points 1 to 4 are MTPV points that will be further explained in section 2.5.

2.4. Operating regions

Fig. 4 depicts different operating modes depending on the motor speed and on the required torque. Γ_{max} is the maximum possible torque for a given maximum thermally-limited current i_{smax}. If i_{smax} is the nominal current, Γ_{max} will be the nominal torque. If the required torque is above Γ_{max} and the motor speed is low, only currents inside the i_{smax} circle are possible, so the current reference generator will output the values of point 1. Let's suppose that the required torque is Γ_{ref} and the motor speed is ω_1. As it can be observed, Γ_{ref} can be obtained by any current contained in the section of the Γ_{ref} curve from point 2, the voltage limitation, to point 6, the maximum current limitation.

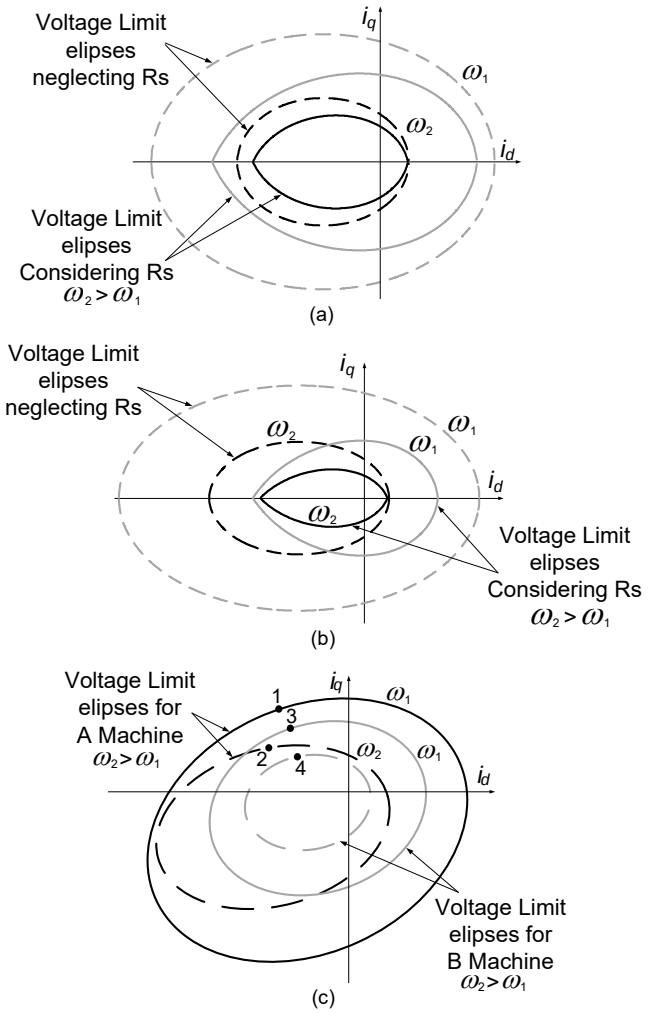

***Fig. 3**. Voltage limits comparison*

(a) A IPMSM in motor operation mode
(b) B IPMSM in motor operation mode
(c) A IPMSM and B IPMSM for the first and fourth quadrants

One of the available current value is the MTPA value, point 3, so it will be chosen as the currents reference.

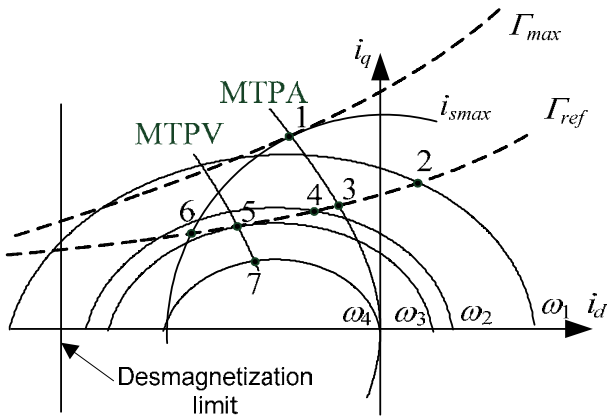

***Fig. 4.** Effect of motor speed on achievable torque references*

When the motor operates at a higher motor speed, ω_2, the same torque can be obtained using the set of currents contained in the segment delimited by point 4 and point 6.

The MTPA point is not accessible, and the current at point 4 becomes the minimum current leading to the desired torque. This region can be denoted as the Optimum Current Region (OCR). As it can be observed, the higher the speed, the thinner the segment of available currents, until ω_3 is reached. At this speed, there is only one current, at point 5, leading to the desired torque. This current provides the maximum torque available at this speed due to voltage limitations. Point 6 is outside the voltage limit for ω_3 and, moreover, the current at point 6 is higher than the current at point 5. Drawing all the current values that lead to the maximum possible torque at each operation speed the Maximum Torque Per Volt (MTPV) path is obtained. If the motor turns at very high speed, let's say ω_4, Γ_{ref} is no longer reachable and the maximum torque will be obtained by the current at point 7 belonging to the MTPV path.

As it can be observed the selected current depends on the intersection of different curves that evolve as the reference torque, motor speed, battery voltage and thermal state of the motor vary. Look Up Tables, though simple to build and easy to use, are not practical with such a wide input dimension so an analytical and compact reference generation is desirable. Next, the MTPV curve and the OCR path will be computed.

2.5. Computing of the MTPV path

The intersection of the constant torque (1) and the Voltage Limit curve (8) is

$$\Gamma(i_q) = Ai_q + Bi_q\left(\frac{-E - Gi_q - \sqrt{Ji_q^{\,2} + Ii_q + K}}{2C}\right) \tag{9}$$

Where

$$A = 1.5\,p\,\phi \tag{10}$$

$$B = 1.5\,p(L_d - L_q) \tag{11}$$

$$C = R^2 + \omega^2 L_d^{\,2} \tag{12}$$

$$D = \mathrm{R}^2 + \omega^2 L_q^{\,2} \tag{13}$$

$$E = 2\omega^2 \phi L_d \tag{14}$$

$$F = 2\phi R|\omega| \tag{15}$$

$$G = 2R|\omega|(L_d - L_q) \tag{16}$$

$$H = \omega^2\phi^2 - V_{SM}^{\,2} \tag{17}$$

$$I = 2EG - 4CF \tag{18}$$

$$J = G^2 - 4CD \tag{19}$$

$$K = E^2 - 4CH \tag{20}$$

Equation (9) gives all the available torque values for any i_q current located at the voltage limit curve. Thus, the maximum torque provided by (9) will be the Maximum Torque Per Volt point for a particular voltage. As torque in (9) depends on current i_q, the MTPV point is obtained computing the derivative of (9) with respect to i_q, see Appendix 6.2. A fourth degree polynomial in i_q is finally obtained and the correct i_q value is retained, (21) for $\omega > 0$ and (22) for $\omega < 0$. Replacing i_q in (8) it is easy to compute i_d as the solution of a second grade equation (23).

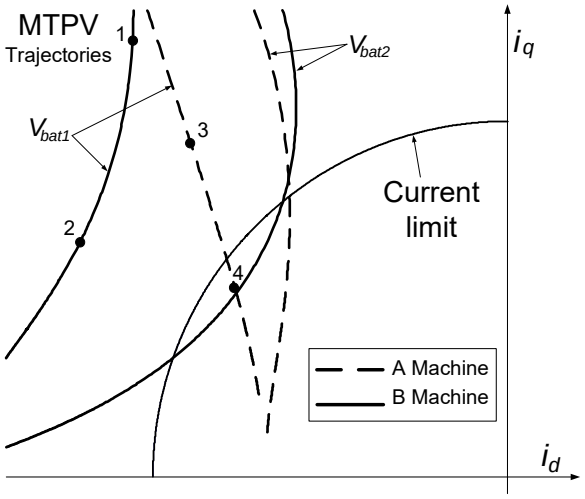

Fig. 5. *MTPV trajectories*

$$i_q = -\frac{c_2}{4c_1} - \frac{h_4}{2} + \frac{\sqrt{h_5 - h_6}}{2} \tag{21}$$

$$i_q = \frac{c_2}{4c_1} + \frac{h_4}{2} - \frac{\sqrt{h_5 - h_6}}{2} \tag{22}$$

$$i_d = \frac{-b - \sqrt{b^2 - 4ac}}{2a} \tag{23}$$

Where c_1, c_2, h_4, h_5, h_6, a, b and c are coefficients that depend on L_d, L_q, ϕ, motor speed and battery voltage, see Appendix 6.2. As each voltage level has a given MTPV point, the MTPV curve is the collection of all MTPV points related to all possible voltage levels.

Expressions (21), (22) and (23) depend on motor parameters (L_d, L_q, ϕ, R, p), the motor speed (ω) and the battery voltage (V_{bat}). Fig. 5 shows the resulting MTPV curves with two battery voltage levels, V_{bat1} = 9*V* and V_{bat2} =6*V*, for both A and B IPMSMs. Points 1 to 4 are the same points as in Fig. 3 (d). As it has been explained previously, as the speed increases, the centre of the ellipse moves to the left and down side of the i_{dq} plane, and the lower the inductance, the larger the displacement. Moreover, this deformation is greater for low battery voltages. Thus, MTPV trajectories for IPMSMs with low inductances operating at low battery voltages differ from the typical MTPV trajectories in literature, as in Fig. 4.

2.6. Computing of the OCR path

The intersection of the required torque with the Voltage Limit Curve, which leads to the OCR path, is obtained by clearing i_q in (1) and replacing it in equation (8). A fourth order polynomial (see Appendix 6.3 for more details) leads to the only logical i_d solution (24).

$$i_d = -\frac{s_2}{4s_1} - \frac{g_4}{2} + \frac{\sqrt{g_5 - g_6}}{2} \tag{24}$$

The standard torque expression (1) provides the torque as a function of *d-q* currents, so once the OCR i_d current is computed, it is straightforward (using (6), i.e. equation (1)

reformulated) to get the required i_q current for a given torque reference.

2.7. Maximum Torque trajectory in the whole speed range

From this point on, explanations will be based on curves obtained using the set of parameters of Table 1 corresponding to the IPMSM under study.

The maximum torque trajectory is determined by the Maximum Current Limit (MCL) and the MTPV curve.

Fig. 6 (a) shows the path of the current providing the maximum possible torque along the whole speed range. Fig. 6. (b) shows the maximum torque-speed curve including the key points from Fig. 6. (a).

As it can be observed, from 0 rpm to ω_{nom} the nominal torque can be achieved and the current reference stays constant at point 1. At ω_{nom} the maximum available voltage is reached so as the speed increases the current moves from point 1 to point 2 along the current limit, and therefore the maximum available torque decreases. At point 2 the MTPV path is attained and the current evolves from 2 to 3 along the MTPV curve. Finally, from 3 on, the maximum torque is given by the MCL again.

Point 2 of Fig. 6. is determined by the intersection of the voltage limit curve (8) with the current limit circle ($i_s = i_{smax}$), leading to a fourth degree polynomial in i_d (see Appendix 6.4 for more details). The logical i_d solution is retained (25) and i_q is obtained through equation (2), using (26) for the first quadrant and (27) for the third quadrant.

$$i_d = -\frac{d_2}{4d_1} - \frac{f_4}{2} - \frac{\sqrt{f_5 - f_6}}{2} \tag{25}$$

$$i_q = \sqrt{i_s^{\,2} - i_d^{\,2}} \tag{26}$$

$$i_q = -\sqrt{i_s^{\,2} - i_d^{\,2}} \tag{27}$$

2.8. Algorithm

The algorithm flowchart is shown in Fig. 7. The basic strategy is to compute the maximum available torque at the operation point and to establish if the reference torque can be reached or not. If it is not possible, the maximum permissible torque is provided, that is, that corresponding to the maximum current limit or to the current at the MTPV curve. If the reference torque is under the maximum one, the best-suited current must be determined using the MTPA or OCR curves.

Fig. 8 (a) shows how the maximum torque is identified. Operating at ω_1, point 1 is the intersection with the maximum available current whereas point 2 is the MTPV value. At ω_2 point 3 depicts the maximum current case and point 4 is the MTPV case. In both speeds, the maximum torque is achieved by the current with the minimum i_d component.

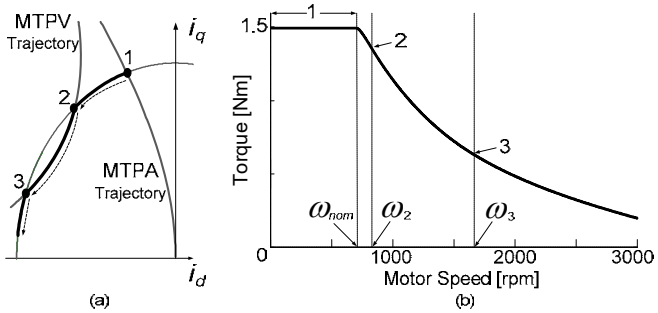

Fig. 6. *Maximum torque trajectory in the full speed range for the IPMSM under test, with a battery voltage of 6V*
(a) in the i_d-i_q plane, (b) in the motor speed-torque plane

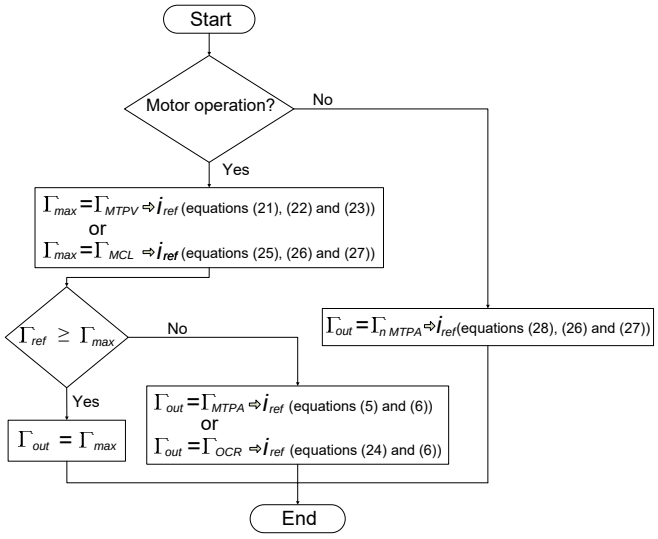

Fig. 7. *Algorithm flowchart*

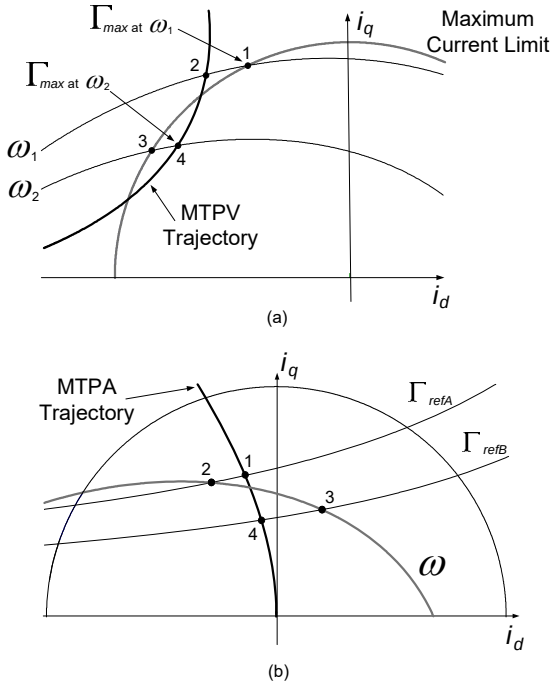

Fig. 8. *Optimum current references*
(a) Maximum torque current vector at high speeds,
(b) Minimum current vectors with two torque references, being $\Gamma_{refA}, \Gamma_{refB} < \Gamma_{max}$

For a given reference torque and speed, if the reference torque is lower than the computed maximum torque, a new computation is needed. Two different cases are represented in Fig. 8 (b). The algorithm computes the MTPA point for the required torque (points 1 and 4) and the intersection between the required torque curve and the voltage limit curve (points 2 and 3). The point that has a lower iq is chosen, that is, point 2 (OCR) for ΓrefA, and point 4 (MTPA) for ΓrefB.

When the machine works in generator mode there is no voltage restriction, so optimum current references are obtained from the intersection of the MTPA trajectory with the current limit (28). In order to compute i_d the algorithm uses (26) for positive speeds and (27) for negative speeds.

$$i_d = \frac{0.25}{(L_d - L_q)}\left(\sqrt{(\phi^2 + 8(L_d - L_q)^2 i_s^2} - \phi\right) \tag{28}$$

3. Simulation and experimental results

The algorithm was implemented in C and included in a Matlab-Simulink S-function in order to perform simulations under different operation modes. This way the algorithm has been validated, including all possible situations (operation in four quadrants) with different models of IPMSM. Fig. 9 reflects the impact of the phase resistance on the behaviour of the IPMSM under study. The battery voltage is only 6V, the motor turns at 1800rpm and the torque reference is 1Nm. The subscript "R" indicates that the resistance has been considered. As it can be observed, when the resistance is considered the maximum available torque of 0.56Nm is easily achieved after a conventional current transient. In the other hand, if the resistance is neglected, an unattainable i_q current reference of 30A is computed. The control tries to cope with this reference but it remains permanently oscillating between the saturated-non saturated states, leading to current and torque oscillations close to the maximum possible torque of 0.56Nm.

Experimental tests have been performed in order to verify the feasibility and effectiveness of the proposed algorithm. The experimental setup (Fig. 10) consists of the IPMSM under test, whose specifications are stated in Table 1 and another IPMSM used as load unit. The tested motor has been connected to a three-phase voltage source inverter, with the switching frequency fixed at 20 kHz and a sampling time period of the current regulation loop of 50μs. In order to measure the rotor speed ω, a contactless magnetic rotary encoder was properly aligned to the tested motor. The torque has been measured with the torque sensor Lorenz Messtechnik GmbH DR-2112-R.

The control system with the algorithm proposed runs on a dSPACE DS1103 real-time platform, with a Power PC 750 GX running at 1GHz. The maximum execution time of the algorithm is 6.93μs (6930 clock periods). Taking into account that a $100\mu s$ sampling and control period is enough in the control of this type of machines, the proposed current generation method is a promising solution on the control of on-board PMSM drives.

Fig. 11 and Fig. 12 show torque and current evolution for 1Nm torque reference and a battery voltage of 6V and 9V respectively, covering all the studied operation modes. Subfigures (a), (b) and (c) show reference and measured values of torque, i_s and i_d and i_q, respectively and subfigure (d) depicts the simulated evolution of i_d and i_q. Motor speed is accelerated during 10 seconds from standby to 2000 rpm in Fig. 11 and up to 2800 rpm in Fig. 12. As it can be observed for both cases, as long as point 2 is not attained, the required torque can be kept and current references evolve from point 1 (MTPA) to point 2 through the OCR region, achieving the torque reference with the optimum current. Thus, the MTPA-OCR identification strategy of section 2.8 (Fig. 8 (b)) is validated. From point 2 to the end of both tests, the algorithm provides the current references belonging to the maximum torque trajectory explained in sections 2.7 and 2.8 (Fig. 8 (a)). In the 6V case, the torque decreases from point 2 to point 3 along the MTPV curve, and beyond point 3 the torque decreases along the MCL path, replicating the evolution shown in Fig. 6. In the 9V case the MTPV curve falls out of the current limit, therefore they do not intersect, so the torque decreases along the MCL path from point 2 on. This way, the proposed MCL or MTPV decision-making strategy is also validated.

4. Conclusions

This work presents, for the first time in literature, analytical expressions that provide MTPA and MTPV current references for all possible motor operation modes without neglecting the phase resistance. An algorithm has been developed that provides the minimum current reference required for each torque reference, thus minimizing the motor heating. Moreover, if the reference torque is not reachable, the algorithm provides the maximum possible torque, thus minimizing the torque error. Contrary to other published works, this work takes into account all the involved variables and all the motor parameters. Computations are held on-line, taking into account the reluctant torque and phase resistances. Analytical motor relationships have been used, with no numerical approximations or simplifications and avoiding the use of look-up-tables. For that sake, analytical expressions of the MTPV trajectory and the intersecting point of the required torque curve with the voltage limit have been obtained, which depend on motor parameters, battery voltage and motor speed. The current reference generator block is motor parameter-sensitive, and those parameters can be adjusted outside the block using a parameter estimation strategy, contrary to look-up-tables based methods. Consequently, the proposed algorithm, assisted by an effective parameter estimator, is a promising solution to enhance IPMSM control performance. The algorithm has been successfully tested in simulation across a wide range of IPMSM models. The feasibility and effectiveness of the proposed control strategy have been experimentally verified on an IPMSM included on an EPS system. In the near future, this work must be linked with parameter estimator strategies in such a way that the best possible behavior is obtained.

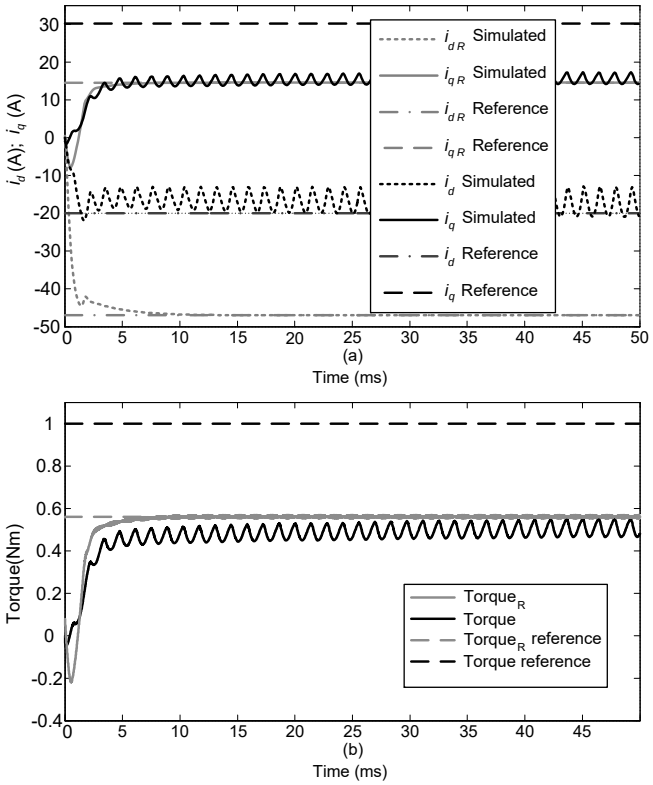

Fig. 9. *Comparison between considering the phase resistance and neglecting it for V_{bat}= 6V and 1800rpm. (a) i_d and i_q references and simulated values (b) Torque references and simulated values*

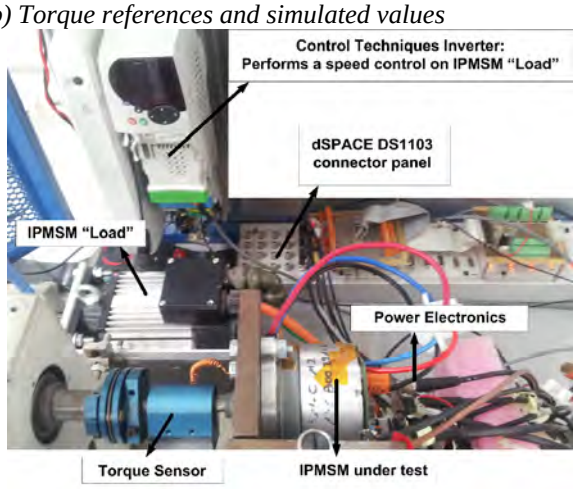

Fig. 10. *Test experimental-rig*

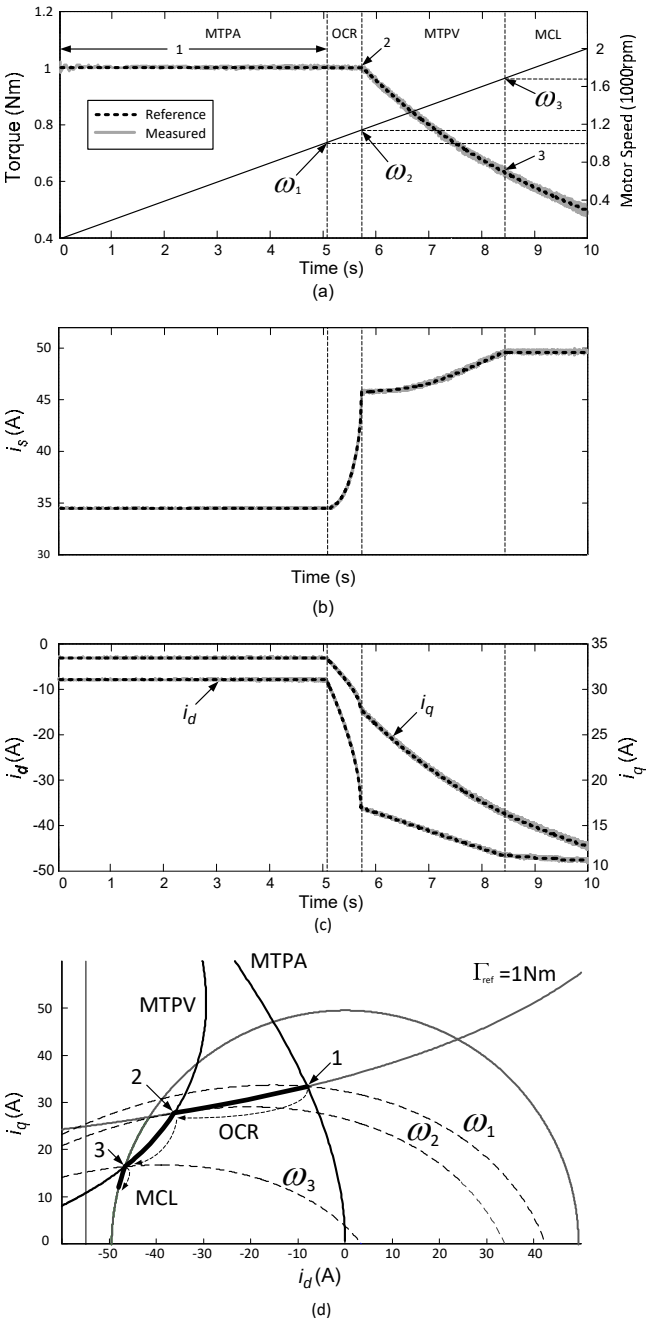

Fig. 11. *Torque and current evolution for 1Nm torque reference and a battery voltage of 6V*

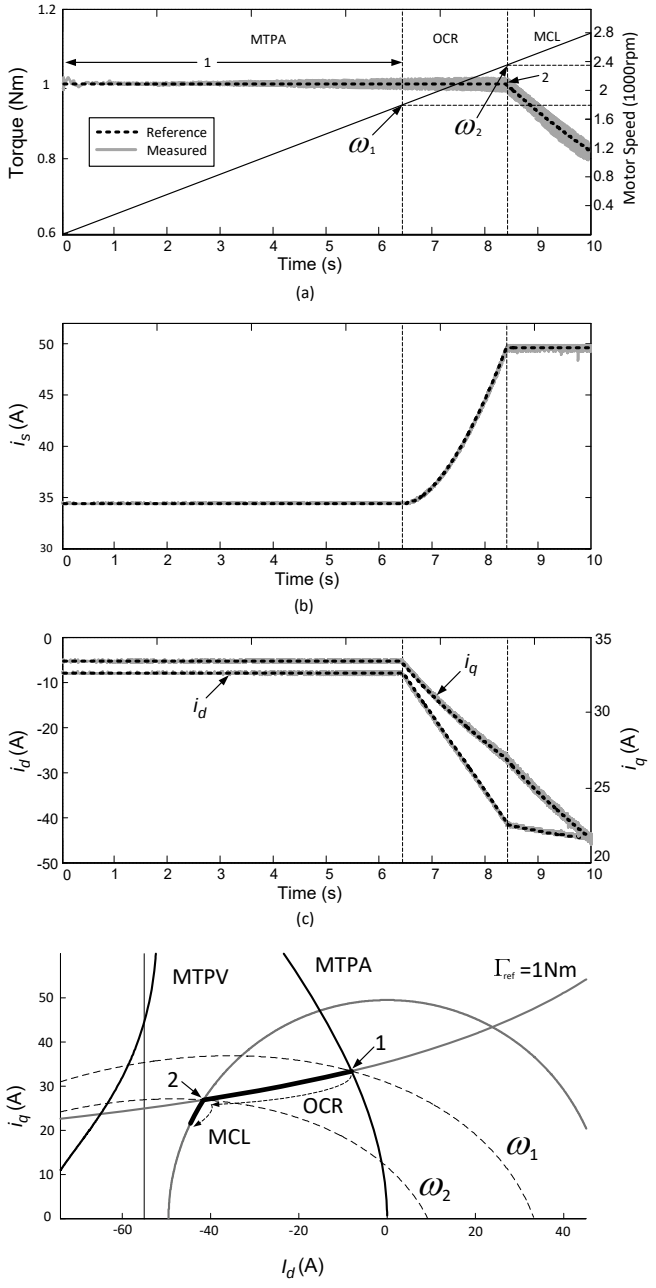

Fig. 12*. Torque and current evolution for 1Nm torque reference and a battery voltage of 9V*

5. References

[1] Morimoto, S., Takeda, Y., Hirasa, T.,Taniguchi, K.: 'Expansion of operating limits for permanent magnet motor by current vector control considering inverter capacity', IEEE Transactions on Industry Applications, 1990V, 26, (5), pp.866-871.

[2] Jahns, T. M.: 'Flux-weakening regime operation of an interior permanent-magnet synchronous motor drive', IEEE Transactions on Industry Applications, 1987, 23, (4), pp. 681-689.

[3] Bianchi, N., Bolognani, S., Zigliotto M.: 'High-performance PM synchronous motor drive for an electrical scooter', IEEE Transactions on Industry Applications, 2001,37, (5), pp. 1348-1355.

[4] Bing Cheng, C., Tesch, T.R.: 'Torque feedforward control technique for permanent-magnet synchronous motors', IEEE Transactions on industrial electronics, 2010, 57, (3), pp.969-366.

[5] Consoli, A., Scelba, G., Scarcella, G., Cacciato, M.: 'An effective energy-saving scalar control for industrial IPMSM drives', IEEE Transactions on industrial electronics, 2013, 60, (9), pp.3658-3669.

[6] Chen, Y. Z., Fang, Y. T., Huang, X. Y., Zhang, J.: 'Torque and flux weakening control with MTPV for interior permanent magnet synchronous motor', IEEE Vehicle Power and Propulsion Conference, Hangzhou, China, Oct 2016, pp.1-5.

[7] Ekanayake, S., Dutta, R., Rahman, M.F., Xiao, D.: 'Direct torque and flux control of interior permanent magnet synchronous machine in deep flux-weakening region', IET Electr. Power Appl., 2018, 12, (1), pp. 98–105.

[8] Huang, S., Chen, Z., Huang, K., Gao, J.: 'Maximum torque per ampere and flux-weakening control for PMSM based on curve fitting', Vehicle Power and Propulsion Conference , Lille, France, Sept 2010, pp. 1-5.

[9] Hu, D., Zhu, L., Xu, L.: 'Maximum torque per volt operation and stability improvement of PMSM in deep flux-weakening region', Energy Conversion Congress and Exposition (ECCE), USA, Raleigh, Sept 2012, pp. 1233 – 1237.

[10] Pan, C.T., Sue, S.M.: 'A linear maximum torque per ampere control for IPMSM drives over full-speed range', IEEE Transactions on energy conversion, 2005, 20, (2), pp.359-366.

[11] Sue, S.M., Pan, C.T.,: 'Voltage-constraint-tracking-based field-weakening control of IPM synchronous motor drives', IEEE Transactions on industrial electronics, 2008, 55, (1) , pp.340-347.

[12] Hoang, K.D., Zhu, Z.Q., Foster, M.: 'Online optimized stator flux reference approximation for maximum torque per ampere operation of interior permanent magnet machine drive under direct torque control', 6th IET International Conference on Power Electronics, Machines and drives, Bristol, UK, March, 2012, pp. B54–B54,

[13] Uddin, M.N., Radwan T.S., Rahman M.A.: 'Performance of interior permanent magnet motor drive over wide speed range', IEEE Transactions on energy conversion, 2002, 17, (1), pp. 79-84.

[14] Morimoto, S., Sanada, M., Takeda, Y.: 'Wide-speed operation of interior permanent magnet synchronous motors with high-performance current regulator', IEEE Transactions on Industry applications, 1994, 30, (4), pp. 920-926.

[15] Bonifacio, J., Kennel, R.: 'Online maximum torque per ampere control of interior permanent magnet synchronous machines (IPMSM) for automotive applications', 8th IET Int. Conf. Power Electron. Mach. Drives, Glasgow, UK, Apr 2016, vol. 10, no. 1, pp. 1–5.

[16] Lei, H.: 'Universal MTPA control for permanent magnet synchronous motor drives', 2nd International Conference on Robotics and Automation Engineering, Shangai, China, Dec 2017, pp.322-326.

[17] Sun, T., Koç, M., Wang, J.: 'MTPA control of IPMSM drives based on virtual signal injection considering machine parameter variations', IEEE Transactions on industrial electronics, 2018, 65, (8), pp.6089-6098.

[18] Lin, F.-J., Liu, Y.-T., Yu, W.-A.: 'Power perturbation based MTPA with an online tuning speed controller for an IPMSM drive system', IEEE Transactions on industrial electronics, 2018, 65, (5), pp.3677-6687.
[19] An, Q., Sun, L.: 'On-line parameter identification for vector controlled PMSM drives using adaptive algorithm', Veh. Power Propuls. Conf. Harbin, China Sep 2008, vol. 0, no. 2, pp. 1–6, 2008.
[20] Phowanna, P., Boonto, S., Konghirun, M.: 'Online parameter identification method for IPMSM drive with MTPA', 18th Int. Conf. Electr. Mach. Syst. Pattaya, Thailand, Oct 2015, pp. 1775–1780.
[21] Dang, D. Q., Rafaq, M. S., Choi, H. H., Jung, J.-W.: 'Online parameter estimation technique for adaptive control applications of interior PM synchronous motor drives', IEEE Trans. Ind. Electron., 2016, 63, (3), pp. 1438–1449.

6. Appendices

6.1. MTPA equations

$$i_d^4 t_1 + i_d^3 t_2 + i_d^2 t_3 + i_d t_4 + t_5 = 0 \tag{29}$$

Where:

$$t_1 = k_4 k_7 k_1 \tag{30}$$

$$t_2 = k_4 k_7 k_2 + k_5 k_7 k_1 \tag{31}$$

$$t_3 = k_3 k_4 k_7 + k_3 k_7 k_1 + k_5 k_7 k_2 - k_6 k_1 \tag{32}$$

$$t_4 = k_3 k_7 k_2 + k_5 k_7 k_3 - k_6 k_2 \tag{33}$$

$$t_5 = {k_3}^2 k_7 - k_6 k_3 - k_4 {\Gamma_{ref}}^2 \tag{34}$$

$$k_1 = \left(L_d - L_q\right)^2 \tag{35}$$

$$k_2 = 2\Phi\left(L_d - L_q\right) \tag{36}$$

$$k_3 = \Phi^2 \tag{37}$$

$$k_4 = 4\left(L_d - L_q\right)^2 \tag{38}$$

$$k_5 = 4\Phi\left(L_d - L_q\right) \tag{39}$$

$$k_6 = \left(\frac{3}{2} p\Phi\right)^2 \tag{40}$$

$$k_7 = \left(\frac{3}{2} p\right)^2 \tag{41}$$

$$i_d = -\frac{t_2}{4t_1} - \frac{p_4}{2} - \frac{\sqrt{p_5 - p_6}}{2} \tag{5}$$

Where:

$$p_1 = 2t_3^3 - 9t_2 t_3 t_4 + 27 t_1 t_4^2 + 27 t_2^2 t_5 - 72 t_1 t_3 t_5 \tag{42}$$

$$p_2 = p_1 \sqrt{-4({t_3}^2 - 3t_2 t_4 + 12 t_1 t_5)^3 + p_1^2} \tag{43}$$

$$p_3 = \frac{{t_3}^2 - 3t_2 t_4 + 12 t_1 t_5}{3t_1 \left(\frac{p_2}{2}\right)^{\frac{1}{3}}} + \frac{\left(\frac{p_2}{2}\right)^{\frac{1}{3}}}{3t_1} \tag{44}$$

$$p_4 = \sqrt{\frac{{t_2}^2}{4{t_1}^2} - \frac{2t_3}{3t_1} + p_3} \tag{45}$$

$$p_5 = \frac{{t_2}^2}{2{t_1}^2} - \frac{4t_3}{3t_1} - p_3 \tag{46}$$

$$p_6 = \frac{-\frac{{t_2}^3}{{t_1}^3} + \frac{4t_2 t_3}{{t_1}^2} - \frac{8t_4}{t_1}}{4p_4} \tag{47}$$

6.2. MTPV equations

$$\frac{d\Gamma(i_q)}{di_q} = a_1 - a_2 i_q - \frac{b_1 {i_q}^2 + b_2 i_q + b_3}{\sqrt{J i_q^2 + I i_q + K}} = 0 \tag{48}$$

Where

$$a_1 = A - \frac{BE}{2C} \tag{49}$$

$$a_2 = \frac{BG}{C} \tag{50}$$

$$b_1 = \frac{BJ}{C} \tag{51}$$

$$b_2 = \frac{3BI}{4C} \tag{52}$$

$$b_3 = \frac{BK}{2C} \tag{53}$$

$$i_q^4 c_1 + i_q^3 c_2 + i_q^2 c_3 + i_q c_4 + c_5 = 0 \tag{54}$$

Where:

$$c_1 = J{a_2}^2 - {b_1}^2 \tag{55}$$

$$c_2 = -2Ja_1 a_2 + I{a_2}^2 - 2b_1 b_2 \tag{56}$$

$$c_3 = J{a_1}^2 - 2Ia_1 a_2 + K{a_2}^2 - b_2^2 - 2b_1 b_3 \tag{57}$$

$$c_4 = I{a_1}^2 - 2Ka_1 a_2 - 2b_2 b_3 \tag{58}$$

$$c_5 = K{a_1}^2 - b_3^2 \tag{59}$$

$$i_q = -\frac{c_2}{4c_1} - \frac{h_4}{2} + \frac{\sqrt{h_5 - h_6}}{2} \tag{21}$$

$$i_q = \frac{c_2}{4C_1} + \frac{h_4}{2} - \frac{\sqrt{h_5 - h_6}}{2} \tag{22}$$

Where:

$$h_1 = 2c_3^3 - 9c_2 c_3 c_4 + 27 c_1 c_4^2 + 27 c_2^2 t_5 - 72 c_1 c_3 c_5 \tag{60}$$

$$h_2 = h_1 \sqrt{-4({c_3}^2 - 3c_2 c_4 + 12 c_1 c_5)^3 + h_1^2} \tag{61}$$

$$h_3 = \frac{{c_3}^2 - 3c_2 c_4 + 12 c_1 c_5}{3c_1 \left(\frac{p_2}{2}\right)^{\frac{1}{3}}} + \frac{\left(\frac{p_2}{2}\right)^{\frac{1}{3}}}{3c_1} \tag{62}$$

$$h_4 = \sqrt{\frac{{c_2}^2}{4{c_1}^2} - \frac{2c_3}{3c_1} + p_3} \tag{63}$$

$$h_5 = \frac{{c_2}^2}{2{c_1}^2} - \frac{4c_3}{3c_1} - p_3 \tag{64}$$

$$h_6 = \frac{-\frac{{c_2}^3}{{c_1}^3} + \frac{4c_2 c_3}{{c_1}^2} - \frac{8c_4}{c_1}}{4p_4} \tag{65}$$

$$i_d^2(R^2+\omega^2L_d^2)+i_d\left(2\omega^2\Phi\mathrm{L_d}+2i_q|\omega|R\left(L_d-L_q\right)\right)+\left(i_qR+\Phi|\omega|\right)^2+\omega^2L_q^2iq^2-V_{SM}^2=0 \quad (66)$$

$$a=R^2+\omega^2L_d^2 \quad (67)$$

$$b=2\omega^2\Phi L_d+2i_q|\omega|R\left(L_d-L_q\right) \quad (68)$$

$$c=\left(i_qR+\Phi|\omega|\right)^2+\omega^2L_q^2iq^2-V_{SM}^2 \quad (69)$$

$$i_d=\frac{-b-\sqrt{b^2-4ac}}{2a} \quad (23)$$

6.3. OCR equations

$$i_d{}^4S_1+i_d{}^3S_2+i_d{}^2S_3+i_dS_4+S_5=0 \quad (70)$$

Where

$$S_1=\left(v_6+v_9\right)v_1 \quad (71)$$

$$S_2=v_6v_2+v_{10}v_1+v_9v_2 \quad (72)$$

$$S_3=v_6v_3-v_8v_4\Gamma_{ref}+v_{11}v_1+v_9v_3+v_{10}v_2+v_{12}v_4\Gamma_{ref}-V_{SM}^2v_1 \quad (73)$$

$$S_4=-v_8v_5\Gamma_{ref}+v_{11}v_2+v_{10}v_3+v_{13}v_4\Gamma_{ref}+v_{12}v_5\Gamma_{ref}-V_{SM}^2v_2 \quad (74)$$

$$S_5=v_7\Gamma_{ref}^2+v_6\Gamma_{ref}^2+v_{11}v_3+v_{13}v_5\Gamma_{ref}-V_{SM}^2v_3 \quad (75)$$

$$v_1=\frac{9}{4}p^2\left(L_d-L_q\right)^2 \quad (76)$$

$$v_2=\frac{9}{2}p\phi\left(L_d-L_q\right) \quad (77)$$

$$v_3=\frac{9}{4}p^2\phi^2 \quad (78)$$

$$v_4=\frac{3}{2}p\left(L_d-L_q\right) \quad (79)$$

$$v_5=\frac{3}{2}p\phi \quad (80)$$

$$v_6=R^2 \quad (81)$$

$$v_7=L_q^2\omega^2 \quad (82)$$

$$v_8=2RL_q\omega \quad (83)$$

$$v_9=L_d^2\omega^2 \quad (84)$$

$$v_{10}=2\omega^2L_d\phi \quad (85)$$

$$v_{11}=\omega^2\phi^2 \quad (86)$$

$$v_{12}=2R\omega L_d \quad (87)$$

$$v_{13}=2R\omega\phi \quad (88)$$

$$i_d=-\frac{S_2}{4S_1}-\frac{g_4}{2}+\frac{\sqrt{g_5-g_6}}{2} \quad (24)$$

Where:

$$g_1=2S_3^3-9S_2S_3S_4+27S_1S_4^2+27S_2^2S_5-72S_1S_3S_5 \quad (89)$$

$$g_2=g_1\sqrt{-4\left(S_3{}^2-3S_2S_4+12S_1S_5\right)^3+g_1^2} \quad (90)$$

$$g_3=\frac{S_3{}^2-3S_2S_4+12S_1S_5}{3S_1\left(\frac{p_2}{2}\right)^{\frac{1}{3}}}+\frac{\left(\frac{p_2}{2}\right)^{\frac{1}{3}}}{3S_1} \quad (91)$$

$$g_4=\sqrt{\frac{S_2{}^2}{S_1a^2}-\frac{2S_3}{3S_1}+p_3} \quad (92)$$

$$g_5=\frac{S_2{}^2}{2S_1{}^2}-\frac{4S_3}{3S_1}-p_3 \quad (93)$$

$$g_6=\frac{-\frac{S_2{}^3}{S_1{}^3}+\frac{4S_2S_3}{S_1{}^2}-\frac{8S_4}{S_1}}{4p_4} \quad (94)$$

6.4. MCL equations

$$i_d^4d_1+i_d^3d_2+i_d^2d_3+i_dd_4+d_5=0 \quad (95)$$

Where

$$d_1=\left(\omega^2\left(L_d^2-L_q^2\right)\right)^2+\left(2R\omega\left(L_q-L_d\right)\right)^2 \quad (96)$$

$$d_2=4\left(L_d^2-L_q^2\right)L_d\omega^4\Phi-8R^2\omega^2\left(L_q-L_d\right)\Phi \quad (97)$$

$$d_3=\left(2L_d(\omega^2\Phi)\right)^2-\left(2R\omega\left(L_q-L_d\right)\right)^2i_s^2+2\omega^2(L_d^2-L_q^2)\left(i_s^2(L_q^2\omega^2+R^2)+\Phi^2\omega^2-V_{SM}^2\right)+(2R\omega\Phi)^2 \quad (98)$$

$$d_4=4Ld\,\Phi\omega^2\left[i_s^2(L_q^2\omega^2+R^2)+\Phi^2\omega^2-V_{SM}^2\right]+(2R\omega)^2i_s^2(L_q-L_d)\,\Phi \quad (99)$$

$$d_5=\left(i_s^2\left(L_q^2\omega^2+R^2\right)+\Phi^2\omega^2-V_{SM}^2\right)^2-(2R\omega\Phi)^2i_s^2 \quad (100)$$

$$i_d=-\frac{d_2}{4d_1}-\frac{f_4}{2}-\frac{\sqrt{f_5-f_6}}{2} \quad (25)$$

Where

$$f_1=2d_3^3-9d_2d_3d_4+27d_1d_4^2+27d_2^2d_5-72d_1d_3d_5 \quad (101)$$

$$f_2=f_1\sqrt{-4\left(d_3{}^2-3d_2d_4+12d_1e\right)^3+f_1^2} \quad (102)$$

$$f_3=\frac{d_3{}^2-3d_2d_4+12d_1d_5}{3d_1\left(\frac{p_2}{2}\right)^{\frac{1}{3}}}+\frac{\left(\frac{p_2}{2}\right)^{\frac{1}{3}}}{3d_1} \quad (103)$$

$$f_4=\sqrt{\frac{d_2{}^2}{4d_1{}^2}-\frac{2d_3}{3d_1}+p_3} \quad (104)$$

$$f_5=\frac{d_2{}^2}{2d_1{}^2}-\frac{4d_3}{3d_1}-p_3 \quad (105)$$

$$f_6=\frac{-\frac{d_2{}^3}{d_1{}^3}+\frac{4d_2d_3}{d_1{}^2}-\frac{8d_4}{d_1}}{4p_4} \quad (106)$$

6.5. Set of paramaters for A IPMSM and B IPMSM

Table 1 Parameters of the A IPMSM

Symbol	Item	Quantity
I_n	Nominal current	49.5A
Γ_n	Nominal torque	1.48Nm
I_{dmax}	Demagnetization limit	-55A
p	Pairs of poles	4
ϕ_m	Magnets flux	4.7mWb
L_d	d-axis inductance	60μH
L_q	q-axis inductance	96μH
R	Resistance	37.5mΩ

Table 2 Parameters of the B IPMSM

Symbol	Item	Quantity
I_n	Nominal current	63.64
Γ_n	Nominal torque	3.3
I_{dmax}	Demagnetization limit	-60A
p	Pairs of poles	7
ϕ_m	Magnets flux	4.35mWb
L_d	d-axis inductance	128.6μH
L_q	q-axis inductance	173μH
R	Resistance	40mΩ